ACS NANO

www.acsnano.org

ARTICLE

Site-Specific Chemistry on Gold Nanorods: Curvature-Guided Surface Dewetting and Supracolloidal Polymerization

Hanyi Duan, Zhenyang Jia, Maham Liaqat, Matthew D. Mellor, Haiyan Tan, Mu-Ping Nieh, Yao Lin, Stephan Link, Christy F. Landes, and Jie He*

Cite This: *ACS Nano* 2023, 17, 12788–12797

Read Online

ACCESS | Metrics & More | Article Recommendations | Supporting Information

ABSTRACT: **Control of interparticle interactions in terms of their direction and strength highly relies on the use of anisotropic ligand grafting on nanoparticle (NP) building blocks. We report a ligand deficiency exchange strategy to achieve site-specific polymer grafting of gold nanorods (AuNRs). Patchy AuNRs with controllable surface coverage can be obtained during ligand exchange with a hydrophobic polystyrene ligand and an amphiphilic surfactant while adjusting the ligand concentration (C_{PS}) and solvent condition (C_{water} in dimethylformamide). At a low grafting density of ≤0.08 chains/nm^2, dumbbell-like AuNRs with two polymer domains capped at the two ends can be synthesized through surface dewetting with a high purity of >94%. These site-specifically-modified AuNRs exhibit great colloidal stability in aqueous solution. Dumbbell-like AuNRs can further undergo supracolloidal polymerization upon thermal annealing to form one-dimensional plasmon chains of AuNRs. Such supracolloidal polymerization follows the temperature−solvent superposition principle as revealed by kinetic studies. Using the copolymerization of two AuNRs with different aspect ratios, we demonstrate the design of chain architectures by varying the reactivity of nanorod building blocks. Our results provide insights into the postsynthetic design of anisotropic NPs that potentially serve as units for polymer-guided supracolloidal self-assembly.**

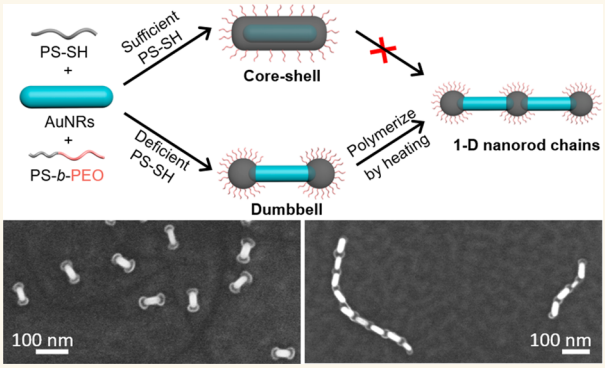

KEYWORDS: *gold nanorods, surface dewetting, self-assembly, nanochains, supracolloidal polymerization*

INTRODUCTION

Nanoparticle (NP) assemblies have been considered as a prototype for artificial molecules/atoms;[1−9] however, the level of their structural complexity and hierarchy is far less than those in molecular or atomic systems.[10,11] Unlike molecules with asymmetric shapes and bond polarization, colloidal synthesis favors high symmetry,[12,13] often leading to isotropic interparticle interactions and the formation of close-packing assemblies.[14,15] As pointed out by Glotzer and others,[16,17] the key structural feature to create directional interaction, but not yet included in those colloidal building blocks, is anisotropy. Despite notable progress in the controlled synthesis of colloidal NPs in terms of their size,[18,19] shape,[20−22] and chemical composition,[23] precise control of interparticle interactions (direction and strength),[2,24−31] even for anisotropic NP building blocks,[32] remains at its early stage in comparison with their covalent counterparts such as atomic or molecular bonding. Among many NP building blocks, there has been growing interest in the self-assembly of plasmonic metal NPs with a localized surface plasmon resonance (LSPR) as a means to harness their collective properties through interparticle near-field coupling.[33−40] While the LSPR peak of individual NPs is sensitive to their shape and size, the LSPR coupling is dominated by the macroscopic packing as an ensemble: e.g., assembly direction and aggregation numbers.[36,37,41,42]

Adding surface ligands to colloidal building blocks provides a meaningful postsynthetic way to design anisotropic metal NPs and potentially guide their self-assembly in a specific

Received: May 2, 2023
Accepted: June 15, 2023
Published: June 21, 2023

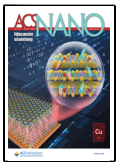

pathway.[2,43−49] A number of methods in the literature have been reported to introduce surface ligands on metal NPs with regioselectivity: e.g., surface facet recognition,[50−52] templated surface grafting,[53,54] and phase segregation of mixed ligands.[55] Together with anisotropic NP topologies, site-specific ligand grafting can provide, or sometimes amplify, the directional interparticle interactions to drive NP assembly in a desired manner.[52,56−63] For example, gold nanorods (AuNRs) are a classic type of anisotropic building blocks having distinct LSPR bands along their transverse and longitudinal directions.[64,65] Without regioselective ligand coverage, AuNRs can pack as clusters with a local preferential direction along their sides;[66,67] however, with site-specific modification with ligands, AuNRs can be organized in an end-to-end fashion that allows their longitudinal LSPR coupling.[68−72] An early example from Kumacheva and co-workers demonstrated that thiol-terminated polystyrene (PS-SH) could preferentially bind with Au (111) facets located at the two ends in tetrahydrofuran (THF),[72] because the grafting density of cetyltrimethylammonium bromide (CTAB) on convex (111) facets was considerably lower as compared to that on flat (110) and (100) facets as the sides of AuNRs. With PS-SH grafted at the two ends of AuNRs, those triblocky AuNRs could mimic the self-assembly of amphiphilic block copolymers (BCPs). Driven by the hydrophobicity of PS, PS-grafted AuNRs could assemble to form rings in a poor solvent of PS. The site-specific grafting is also impacted by the binding motifs as reported by the Murphy group.[51] Thiol-terminated poly(ethylene oxide) (PEO-SH) would replace CTAB on the entire surface of AuNRs; however, the disulfide form (PEO-S-S-PEO) led to selective CTAB replacement only at the two ends of AuNRs.

Recent studies suggest that the use of polymer ligands offers a promising solution to break the symmetry of plasmonic metal NPs driven by surface dewetting of polymer ligands upon reduction of solvent quality.[42,73−76] Under ligand deficiency conditions, hydrophobic polymer ligands can form anisotropic surface patches, i.e., partially dewetting the surface of isotropic metal NPs. These anisotropically patched NPs have directional interparticle interactions that guide the assembly of the plasmonic NP building blocks into hierarchical superstructures not feasible previously.[77−79] While the affinity of the binding motifs to different facets is important, the shape complexity of anisotropic NPs, e.g., local surface curvature of anisotropic NPs,[52,57] may enable the interplay of surface energy by varying the solvent quality. Synthesis of water-soluble patchy AuNRs with polymers, however, is technically challenging because their anisotropic structures are sensitive to thermal heating.[80] In this study, we demonstrate a ligand deficiency exchange method to carry out site-specific chemistry on AuNRs. Using single-crystalline AuNRs with symmetry-equivalent (310) surface facets as the lateral and end planes,[81] we showed that the ligand coverage of hydrophobic PS-SH on AuNRs was solely dependent on the concentration of PS-SH (Figure 1a). With the interplay of hydrophobicity-driven surface dewetting and the local surface curvature, polymer-grafted AuNRs evolved from a complete core−shell to a defective core−shell to an end-selectively patched dumbbell (Figure 1b−d). Those dumbbell-like structures were water-soluble with a purity of >94% (Figure 1b). AuNRs with dumbbell patches could act as difunctional monomers to undergo supracolloidal polymerization and generate one-dimensional (1-D) chains with controllable interparticle distance upon thermal annealing

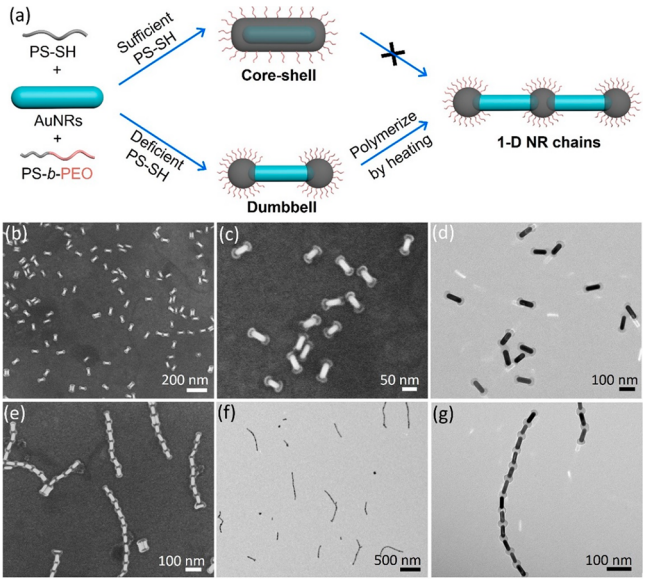

Figure 1. (a) Ligand sufficiency or deficiency exchange on AuNRs to form different surface coverages. (b−d) Electron microscopy characterization of nanorod dumbbells prepared at $C_{PS\text{-}SH}$ = 2.1 μM and C_{water} = 12 vol % in DMF: SEM images (b, c) and TEM image (d) of dumbbell-like AuNRs. (e−g) Electron microscopy characterization of nanorod chains prepared at $C_{PS\text{-}SH}$ = 2.1 μM and C_{water} = 9 vol %: SEM (e) and TEM images (f, g) of nanorod chains.

(Figure 1e−g). We systematically studied polymerization kinetics under different solvent conditions where the temperature−solvent superposition principle could be applied. Those plasmonic 1-D chains with controllable interparticle distance showed length-dependent plasmon coupling along the longitudinal direction. This robust system also allowed us to carry out colloidal copolymerization of two different building blocks that controls the chain topologies and architectures. Those findings provide insights into the design of surface anisotropy on NP building blocks and their polymer-guided supramolecular-like self-assembly.

RESULTS AND DISCUSSION

Ligand Deficiency Exchange of AuNRs. CTAC-capped AuNRs (59.4 × 15.9 nm; Figure S1) were synthesized using a method reported by Murray et al.[81] The transverse and longitudinal LSPR bands of as-synthesized AuNRs in water are at 509 and 767 nm, respectively. To prepare patchy AuNRs, PS_{169}-SH (M_n = 17.6 kg/mol, PDI = 1.2; Figure S2) was used as a ligand, and amphiphilic BCP polystyrene-*block*-poly(ethylene oxide) (PS_{40}-*b*-PEO_{114}, M_n = 9.2 kg/mol, PDI = 1.1) was used as a surfactant to stabilize the nanostructures in water.[42] In a typical synthesis procedure, preconcentrated AuNRs (1.54 mg) were quickly added into 2 mL of DMF containing PS_{165}-SH (concentration range of 5.7−0.71 μM) and PS_{40}-*b*-PEO_{114} (54 μM). After sonicating for 3 min, the solution was incubated at room temperature for 4 h. Afterward, 9 vol % of H_2O (C_{Water}) was added to the above solution to quench the grafting process followed by thermal annealing at 90 °C for 20 min. After cooling to room temperature, the solution was diluted with 10 mL of water containing 25 mM of CTAC and purified by centrifugation. The final AuNRs were dispersed and stored in water at a concentration of 0.14 mg/mL.

https://doi.org/10.1021/acsnano.3c03929
ACS Nano 2023, 17, 12788−12797

Figure 2 shows the transmission electron microscopy (TEM) and scanning electron microscopy (SEM) images of

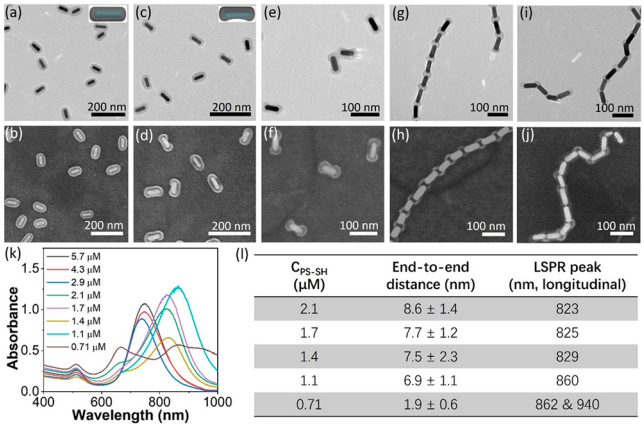

C_{PS-SH} (μM)	End-to-end distance (nm)	LSPR peak (nm, longitudinal)
2.1	8.6 ± 1.4	823
1.7	7.7 ± 1.2	825
1.4	7.5 ± 2.3	829
1.1	6.9 ± 1.1	860
0.71	1.9 ± 0.6	862 & 940

Figure 2. TEM and SEM images of patchy AuNRs prepared at different C_{PS-SH}: (a, b) C_{PS-SH} = 5.7 μM; (c, d) C_{PS-SH} = 4.3 μM; (e, f) C_{PS-SH} = 2.9 μM; (g, h) C_{PS-SH} = 2.1 μM; (i, j) C_{PS-SH} = 0.71 μM. C_{water} = 9 vol % in all cases. (k) UV−vis spectra of patchy AuNRs prepared at different C_{PS-SH}. (l) Summarization of the end-to-end distance (d) and LSPR peak of nanorod chains prepared at five different C_{PS-SH}. The end-to-end distance of AuNRs was the statistical average from >200 particles.

patchy AuNRs prepared under different concentrations of PS_{169}-SH (C_{PS-SH}) in the range of 0.71−5.7 μM. There are clearly morphological transitions when decreasing the concentration of PS_{169}-SH. At C_{PS-SH} = 5.7 μM, the TEM image in Figure 2a shows core−shell nanostructures, where the dark gold core was surrounded by a light polymer layer. The shell thickness was 12.2 ± 1.2 nm (Figure S3), and the entire surface of AuNRs was covered by polymers. The contrast between AuNRs and the polymer was reversed in the corresponding SEM image (Figure 2b). The longitudinal LSPR band of the core−shell structure was located at 750 nm, while the transverse band stayed unchanged. With C_{PS-SH} down to 4.3 μM, incomplete core−shell nanostructures with an open patch at the lateral side were seen in TEM and SEM images, as shown in Figure 2c,d. The open patch was attributed to the dewetting of polymer ligands under deficiency conditions, as the area of the open patch increased when further lowering C_{PS-SH} (Figure S4). Thermogravimetric analysis (TGA) revealed that the overall grafting densities of PS were 0.17 and 0.08 chains/nm^2 at C_{PS-SH} values of 5.7 and 4.3 μM, respectively (Figure S5 and Table S1). This suggests that the surface dewetting of PS_{169}-SH occurred approximately at a grafting density of 0.08 chains/nm^2, close to the reported values (0.10 chains/nm^2) for spherical AuNPs.[74,75] The surface dewetting was presumably driven by the change in solvent quality for PS_{169}-SH grafted AuNRs in the mixture of DMF/water. PS_{169}-SH, instead of core−shell coverage on AuNRs, would segregate or dewet the surface of AuNRs to minimize the interface of the solvent. Phase segregation is only possible at a low grafting density where the entropic repulsion among bound ligands is minimum.

The surface curvature of AuNRs played an essential role in determining the regioselectivity of the polymer ligands. PS_{169}-SH favorably segregated to the two ends of AuNRs at its low concentration range. Upon further decreasing C_{PS-SH} to 2.9 μM, the coverage on the lateral sides continued decreasing until polymer domains were only present on the two ends (Figure 2e,f). The longitudinal LSPR band of such nanostructures was blue-shifted to 739 nm, presumably due to less polymer coverage. The thickness (along the AuNR longitudinal direction) and length (along the AuNR transverse direction) of polymer domains were 11.0 ± 1.4 and 36.4 ± 2.5 nm (Figure S6), respectively. This thickness is similar to that of core−shell AuNRs prepared at C_{PS-SH} = 5.7 μM (12.2 ± 1.2 nm, Figure S3). As CTAC-capped AuNRs have symmetry-equivalent (310) surface facets,[81] the phase segregation of PS_{169}-SH is unlikely to be determined by the binding strength on different facets. Given the difference in surface curvature at the lateral and end planes, the attachment of polymer domains at the two ends would lead to a smaller interface for polymers and solvent.

When C_{PS-SH} reached ≤2.1 μM, AuNRs formed 1-D chains (Figure 2g−j and Figure S4). At C_{PS-SH} = 2.1 μM, TEM and SEM images clearly show polymerized AuNRs interlinked by polymer domains. The formation of a 1-D nanochain was also confirmed spectroscopically. The UV−vis spectrum showed that the longitudinal LSPR band was red-shifted to 823 nm due to the end-to-end plasmon coupling of AuNRs (Figure 2k), which is indicative of nanochain formation. With the further decrease of C_{PS-SH}, there was a clear change in the end-to-end distance (d) between adjacent AuNRs (or average interparticle distance of adjacent AuNRs, Figure 2j). At C_{PS-SH} = 0.71 μM, AuNRs were very close to each other, and d decreased to 1.9 ± 0.6 nm. The end-to-end distance (d) between adjacent AuNRs in chains was analyzed at different concentrations of PS_{169}-SH (Figure 2l). d decreased with C_{PS-SH}, which can be attributed to the low grafting density of PS_{169}-SH. TGA results (Figure S5 and Table S1) indicated that the tip grafting density decreased from 0.25 to 0.09 chains/nm^2 when C_{PS-SH} decreased from 2.1 to 0.71 μM. Note that since the lateral side of AuNRs was exposed in the chain condition, our grafting density was estimated from the surface area at the two ends of AuNRs (see details in Supporting Information). When d is much smaller than the end-to-end distance of PS_{169}-SH, it is likely due to the chain redistributed along the outer surface to interact with the BCP.[26] The shorter distance resulted in strong coupling of the longitudinal plasmon band of AuNRs. The LRSP had a red shift to 940 nm in the case at C_{PS-SH} = 0.71 μM. It is noteworthy that patchy AuNRs and nanorod chains are water-soluble due to the presence of the BCP surfactant PS_{40}-b-PEO_{114} at the two ends and CTAC at the lateral facets. Our control experiment verified that the supplementary CTAC is of vital importance to maintain the stability of dumbbell-like AuNRs and nanorod chains. Without the addition of CTAC before centrifugation, the nanorod chains precipitated out from the water in 30 min after purification. Thus, it is reasonable to assume that the exposed lateral facets of AuNRs are still covered by CTAC (also see below the study of the surface coverage). The water solubility of patchy AuNRs and nanorod chains is a result from the coexistence of CTAC and amphiphilic PS_{40}-b-PEO_{114} that is different from core−shell structures, where water stability solely comes from the hydrophilic PEO corona.

The results at different C_{water} and C_{PS-SH} are summarized into a phase-like diagram as given in Figure 3 (see more TEM images in Figures S7−S12). Three different nanostructures of AuNRs, denoted as core−shell, dumbbell, and chain, can be yielded by varying C_{water} and C_{PS-SH}. The core−shell structures are seen at the top of the diagram, as a higher C_{PS-SH} causes a

https://doi.org/10.1021/acsnano.3c03929
ACS Nano 2023, 17, 12788−12797

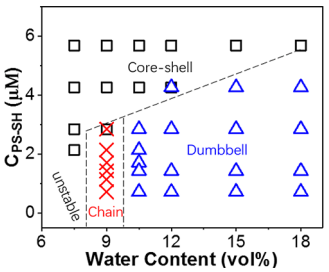

Figure 3. Phase-like diagram of patchy AuNRs obtained at various C_{PS-SH} and C_{water}: core−shell (rectangles), dumbbell (triangles), and chain (cross marks). AuNRs shown in the left bottom corner with low C_{PS-SH} and/or C_{water} are not stable during ligand deficiency exchange.

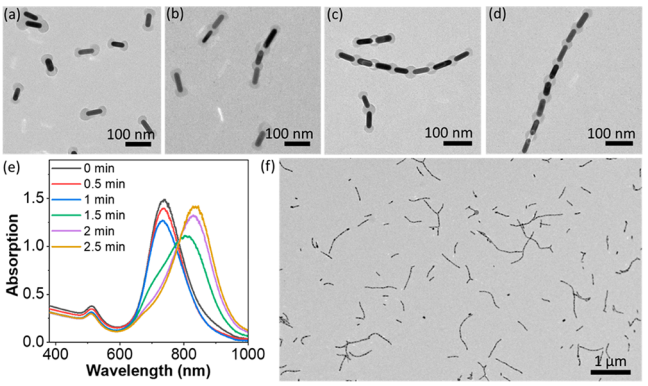

Figure 4. (a−d) TEM images of patchy AuNRs (prepared at C_{PS-SH} = 1.4 μM and C_{water} = 9 vol %) at different thermal annealing times: (a) 0.5 min, (b) 1 min, (c) 1.5 min, (d) 2.5 min. (e) Monitoring the formation of AuNRs chain during thermal annealing at 90 °C using UV−vis spectroscopy. (f) Low-magnification TEM image of nanorod chains after annealing for 2.5 min.

higher grafting density of PS_{169}-SH; thus, symmetrical surface coverage of polymer ligands is observed. At a low C_{PS-SH} and a high C_{water}, dumbbell-like AuNRs with polymer domains selectively attached at the two ends of AuNRs are obtained. Those patchy AuNRs are a result of complete phase separation of C_{PS-SH}. A higher water content tends to prefer the dumbbell nanostructures rather than core−shell, giving the boundary line between core−shell and dumbbell a positive slope, since the poor solvent quality would increase the interfacial energy of polymer ligands and solvents. At C_{PS-SH} of 4.3 μM, the morphology could vary from core−shell to a core−shell/dumbbell mixture and dumbbell upon increasing C_{water} from 9 to 18 vol %. A higher water content would stop the polymerization of dumbbell-like AuNRs to form chains. This is likely because the thermal annealing at 90 °C did not "activate" the PS domains at the two ends of AuNRs in a DMF/water mixture with a high amount of water (see below). Nanorod chains would only form at a very narrow window of $C_{water} \approx 9$ vol %.

Time-Dependence Study: Temperature−Solvent Superposition. To gain mechanistic insights into the formation of nanorod chains, the time-dependence study of supracolloidal polymerization was carried out with UV−vis spectroscopy and TEM by taking advantage of longitudinal plasmon coupling. We first carried out the ligand deficiency exchange in DMF at C_{water} = 9 vol % and C_{PS-SH} = 1.4 μM as described previously without thermal annealing. It is surprising that nearly all modified AuNRs in the solution mixture were dumbbell-like (98%, Figure S13). Its initial LSPR peak appeared at 739 nm, in close agreement with that of dumbbell-like AuNRs. Upon annealing in an oil bath preheated at 90 °C, the LSPR peak had a large red shift after 1.5 min to 805 nm, indicating the end-to-end polymerization of those end-capped dumbbell-like AuNRs. After 2.5 min, the LSPR peak red-shifted to 835 nm, close to that given in Figure 2. We used TEM to characterize the intermediates by quenching the samples with water (Figure 4a−d). Figure 4a shows the nanostructures at 0.5 min. ∼90% of AuNRs were dumbbell-like, and a few dimers could also be seen in the TEM image with a fraction as low as 9% (Figure S14). At 1 min, some multimers can be seen under TEM (Figure 4b), indicating the ongoing growth, but the fraction of single dumbbell-like AuNRs was still as high as 81%. The low monomer conversion agrees with UV−vis spectra, where no red shift of the LSPR peak was observed (Figure 4e). A pronounced transition was seen after 1.5 min. The UV−vis spectrum has a clear peak appearing at 805 nm, indicating the formation of short nanorod chains, while the shoulder peak of dumbbell-like AuNRs is still visible. The TEM images in Figure 4c and Figure S14 confirm that short chains were formed with a dramatic decrease of single dumbbell-like AuNRs (∼22%). After 2 min, the LSPR peak shifted to 830 nm, and the further increase of annealing time would have a minimum impact on their LSPR peaks. TEM images in Figure 4d,f indicate the formation of long nanorod chains of up to micrometers (>20 AuNRs in a single chain). The average degree of polymerization (DP) of nanorod chains increased with polymerization time, as summarized in Figure S14. After polymerization for 2.5 min, the average chain length was 8.0 ± 5.6 with a polydispersity index of 1.6.

The results of kinetic measurement reveal that the structural transition of dumbbell-like AuNRs to nanorod chains is strongly temperature-dependent. At room temperature, dumbbell-like AuNRs are capped by the BCP, PS_{40}-*b*-PEO_{114}, where the PEO corona stabilizes those patchy AuNRs and simultaneously prevents the growth of interparticle assemblies. When AuNRs are annealed with site-specifically-grafted polymers, the dynamics of such systems will increase dramatically. We attribute these dynamics to the change in the polymer solubility (mainly for the PS block). The increase of PS solubility will destabilize dumbbell-like AuNRs with the partial removal of PS_{40}-*b*-PEO_{114}, as the hydrophobic cores (PS_{ligand}-PS_{BCP}) could be weakened when the solvent quality changed accordingly.[73,74,82] The exposed PS end of dumbbell-like AuNRs, in the absence of the PEO block, becomes thermodynamically unfavorable, and those activated difunctional AuNRs would assemble with each other to propagate (Figure 5a). The activation of dumbbell-like AuNRs was also evidenced by the initial change of the longitude LSPR peak, where a slight blue shift was observed from 739 to 734 nm in the first 60 s of thermal annealing. This shift was also confirmed in different solvent compositions (Figure 5b). We attribute this blue shift to the resolvation of polymer domains where the refractive index of the solvent (1.40) was lower than that of PS (1.59). Additionally, the formation of chains is not only driven by minimizing the interface of PS ligands with solvents but also limited by electrostatic repulsion among AuNRs. Therefore, the end-to-end polymerization of dumbbell-like AuNRs dominates with minimum side-to-side polymerization. Since the surface energy gain through

https://doi.org/10.1021/acsnano.3c03929
ACS Nano 2023, 17, 12788−12797

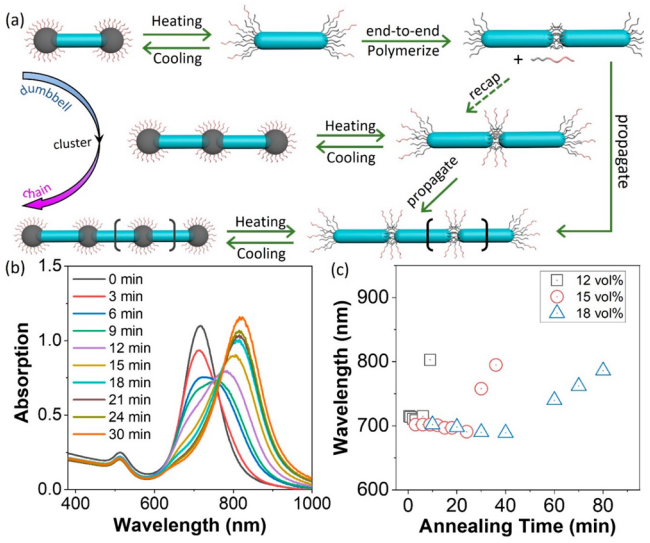

Figure 5. (a) Scheme showing the proposed supracolloidal polymerization mechanism. (b) UV−vis spectra showing the formation of AuNRs chains (prepared at $C_{PS\text{-}SH}$ = 1.4 μM, C_{water} = 9 vol %) during thermal annealing at 80 °C. (c) Plotting the longitudinal plasmon band of patchy AuNRs (prepared at $C_{PS\text{-}SH}$ = 1.4 μM) at different C_{water} against annealing time during thermal treatment at 100 °C.

polymerization is largely negative, the supracolloidal polymerization occurs much faster, as compared to the self-assembly of those NP building blocks.[60] However, the kinetic barrier would be the initial removal of PS_{40}-*b*-PEO_{114} that is controlled by the solubility of PS.

To confirm the supracolloidal polymerization mechanism, we carried out three sets of control experiments. First of all, dumbbell-like AuNRs prepared at different water contents (e.g., 12−18 vol %) with $C_{PS\text{-}SH}$ = 1.4 μM were annealed at a higher temperature. UV−vis spectroscopy was again used to monitor the polymerization kinetics. At 100 °C, all three samples prepared at C_{water} of 12, 15, and 18 vol % water content could polymerize, but their kinetics were very different (Figure S15). For example, the transition time (t_{trans}) from dumbbell-like AuNRs to nanorod chains, defined by the abrupt increase of their LSPR peak, is about 9 min at C_{water} of 12 vol%, while t_{trans} increased to 36 and 80 min for C_{water} of 15 and 18 vol %, respectively (Figure 5c). Second, we investigated the supracolloidal polymerization of dumbbell-like AuNRs at 80 °C with C_{water} of 9 vol % (Figure 5b). t_{trans} is about 12 min, as compared to 90 s measured at 90 °C. Lastly, the BCP of PS_{40}-*b*-PEO_{114} has nearly no role in supracolloidal polymerization, but stabilizes the final nanostructures. We varied the BCP concentration in the range of 0.05 mg/mL (5.4 μM) to 1 mg/mL (108 μM) at C_{water} of 9 vol % and $C_{PS\text{-}SH}$ of 1.4 μM. Nanorod chains were obtained in the broad range of the BCP concentration (Figure S16). These results signify that (i) the nanorod chains are indeed evolved from dumbbell-like AuNRs through end-to-end polymerization and (ii) the temperature and solvent play a crucial role in governing the dynamics of polymer domains. The dumbbell-to-chain transition can be concluded as a longer time is needed at a higher water content at the same annealing temperature or less time is needed at a higher annealing temperature with the same water content. In other words, the supracolloidal polymerization follows the temperature−solvent superposition principle.

Surface Coverage Identification. We then investigated whether the surface coverage of AuNRs, by PS_{169}-SH, is changed during the dumbbell-to-chain structural transition since Au-thiolate coordination is known to be unstable at high temperature. We used the seed-mediated growth of palladium (Pd) on the lateral facets of AuNRs.[83] Both dumbbell-like AuNRs and nanorod chains can be used as seeds to template the growth of Pd by taking advantage of the exposed lateral sides (Figure 6a). Figure 6b shows the TEM image of

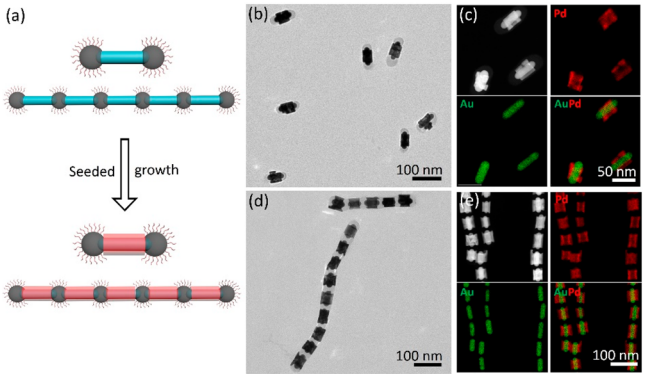

Figure 6. (a) Scheme showing selective Pd growth to form coaxial Pd@AuNR. (b, c) TEM image (b) and HADDF and EDX mapping (c) of dumbbell-Pd@AuNRs. (d, e) TEM image (d) and HADDF and EDX mapping (e) of Pd@AuNR chains.

dumbbell-Pd@AuNRs using Na_2PdCl_4 as a precursor and ascorbic acid (AA) as a reductant. Pd selectively grew on the side of the AuNRs as a uniform shell. The high angle annular dark field (HAADF) and energy-dispersive X-ray spectroscopy (EDX) mapping images (Figure 6c) further confirmed that the growth of Pd only occurred on the lateral side of AuNRs due to the capped polymer domain tips. The thickness of the Pd layers is around 7.2 nm. The Pd layer did not fully cover the lateral side, where some polymer ligands reside on. We estimated the surface Pd coverage of AuNRs, defined as the length ratio l_{Pd}/l_{AuNR}, to be 0.64; that is, roughly 38% of the AuNR surface was covered by polymer ligands. Moreover, the growth of Pd fully wetted the surface of AuNRs, unusual in the case of templated secondary growth of Pd on Au.[42,74,84] This was attributed to the high index (310) facets of AuNRs, overcoming the lattice mismatch of Au and Pd to generate uniform shells. The plasmonic properties of dumbbell-Pd@AuNRs changed dramatically after Pd coating due to plasmon damping. The intensity of the longitudinal band decreased by 80% as compared to dumbbell-like AuNRs, while the transverse band was nearly unidentifiable due to the close contact with Pd (Figure S17). In addition, the seed-mediated growth could be performed with $HAuCl_4$ to grow the coaxial Au on the lateral facets. The longitudinal plasmon band blue-shifted due to the increased diameter of the grown AuNRs, producing a reddish solution (Figure S18).

Similar seed-mediated growth was carried out using nanorod chains as seeds, leading to the asymmetric but coaxial Pd growth as summarized in Figure 6d. Pd domains grew only on the exposed surface of individual AuNRs. Each of them was well-separated by polymer domains at the end of AuNRs. HAADF and EDX mapping images (Figure 6e) confirm that uniform Pd shells completely formed on the side of AuNRs. The chain morphology was not changed after growth, and the polymer domains were preserved at the junction of adjacent

https://doi.org/10.1021/acsnano.3c03929
ACS Nano 2023, 17, 12788−12797

AuNRs. A similar Pd thickness of 7.6 nm was observed at the same precursor feeding amount. The surface Pd coverage of nanorod chains is approximately 0.64, nearly identical with that of dumbbell-like AuNRs. We, therefore, deduced that AuNRs in the forms of chains and dumbbells have the same surface coverage. This result also aligns with our supracolloidal polymerization mechanism, where polymer ligands are not dynamically removed from the two ends of AuNRs.

Plasmonic Chains. We further investigated the shape and chain length dependence of the plasmonic properties of nanorod chains. In view of their length heterogeneity in the ensemble in solution, correlated measurements of single-particle hyperspectral dark field scattering and electron microscopy were utilized.[85] Hyperspectral dark field imaging resolves this heterogeneity by producing a spectrum for every assembly in a given field of view.[85,86] Nanorod chains shown in Figure S11i with an end-to-end distance of 7.7 ± 1.2 nm were studied, and their spectral changes with respect to chain lengths were analyzed.

As nanorod chains grow in an end-to-end fashion, the scattering peak shows an obvious shift along with the increase of scattering peak intensity due to the near field plasmon coupling. Figure 7a,b depicts the SEM images of a dimer and a heptamer of AuNRs, respectively, and their correlated scattering spectra are plotted in Figure 7c. A clear red shift from 670 to 736 nm can be observed as the AuNR chain elongates, due to the in-phase coupling of AuNRs along the longitudinal axis.[87,88] The peak intensity increases by 3-fold. This trend holds for the entire length distribution of AuNR assemblies, where the scattering peak shifts to a longer wavelength with the number of AuNRs (Figure 7d). However, the red shift of the resonance wavelength will diminish and eventually plateau with additional AuNRs due the saturation of electronic interactions between AuNR components in the assembly (Figure S19).[89] Notably, a broader LSPR distribution is observed for the dimer and trimer assemblies. This is likely due to the greater orientation dependence in these structures as reported previously.[87]

Copolymerization: Reactivity Ratio of AuNRs. Taking inspiration from the classic polymerization of organic monomers, we further used NP mixtures with different sizes to study the reactivity of dumbbell-like AuNRs (Figure 8a). We first synthesized another set of longer AuNRs with a length of 99.8 nm and a diameter of 56.1 nm (Figure S20). Their surface dewetting showed a similar trend where the polymer domains capped the two ends of AuNRs at $C_{PS\text{-}SH}$ of 0.28 μM (Figure S21). Those two difunctional dumbbell-like AuNRs (AuNR-1 99.8 × 56.1 nm and AuNR-2 59.4 × 15.9 nm) were mixed in DMF at different feeding ratios ($f_1 = N_{AuNR\text{-}1}/N_{AuNR\text{-}1+AuNR\text{-}2}$, where N_{AuNR} is the number of corresponding AuNRs). After adding 9 vol % of water, the solution mixture was annealed at 90 °C for 20 min. Those two different dumbbell-like AuNRs copolymerized to form nanorod chains with random sequences, as revealed in TEM (Figures 8b–e). Longer AuNRs would tether to the end of chains or behave like a branch point when the feeding ratio (f_2) of AuNR-2 was below 0.2. The branching could be understood as a diameter mismatch of the two AuNRs. When increasing the feeding ratio (f_2) of AuNR-2 to 0.307, the chain structures resemble random copolymers as displayed in Figure 8e.

The molar fraction of AuNRs in nanorod chains (F_1) or feed (f_1) could be analyzed from low-magnification TEM images (Figures S22–S25). The copolymer composition (F_1) was

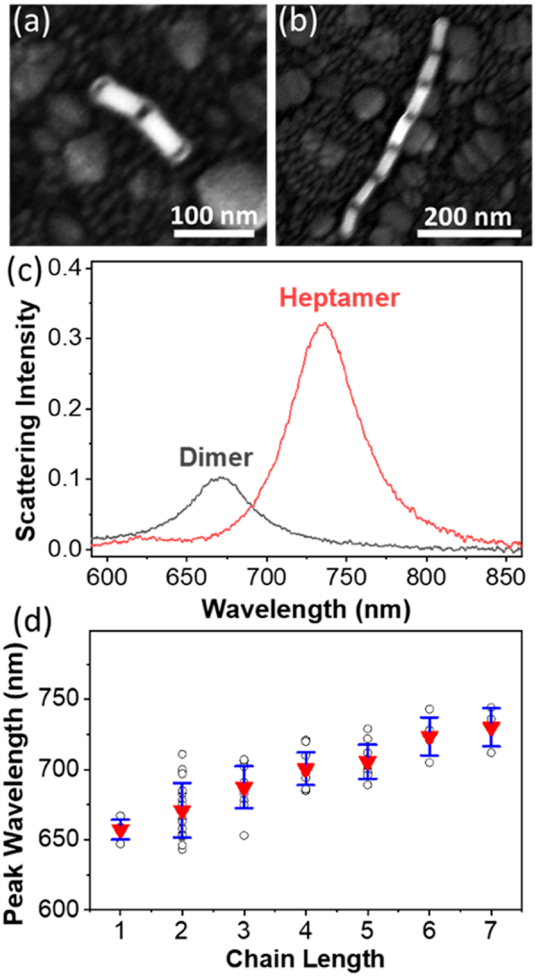

Figure 7. (a, b) SEM images of a dimer and a heptamer AuNR assembly for correlated measurements of single-particle scattering. The interparticle distance between AuNRs was 7.7 ± 1.2 nm. (c) Representative scattering spectra of AuNR assemblies depicted in (a) and (b), respectively. The peak wavelengths were observed at 670 and 736 nm for the dimer and heptamer, respectively. (d) LSPR peak wavelength of nanorod assemblies vs chain length (the number of AuNRs per chain). Red triangles indicate the median resonance wavelength, and blue lines indicate the interquartile range of all measured data.

further plotted against the feeding ratio (f_1) and fitted by a classic copolymerization theory[90]

$$F_1 = \frac{r_1 f_1^2 + f_1 f_2}{r_1 f_1^2 + 2 f_1 f_2 + r_2 f_2^2} \quad (1)$$

where r_i, f_i, and F_i stand for the reactivity ratio, the molar fraction of feeding, and the molar ratio in chains of AuNR-i, respectively. Our four data points fit very well with the copolymerization model, although the dumbbell-like AuNRs obviously have different diffusion coefficients. The fitting results showed that r_1 and r_2 are 7.1 and 4.4, respectively. These high reactivity ratios demonstrate that both AuNR-1 and AuNR-2 had a higher tendency to polymerize themselves rather than to each other. This is consistent with the sequential structures as observed in TEM. We assume that the structural mismatch of the two AuNRs is mainly responsible for the sequential copolymerization. Although AuNR-2 has a much slower diffusion rate than AuNR-1, its homopolymerization

https://doi.org/10.1021/acsnano.3c03929
ACS Nano 2023, 17, 12788–12797

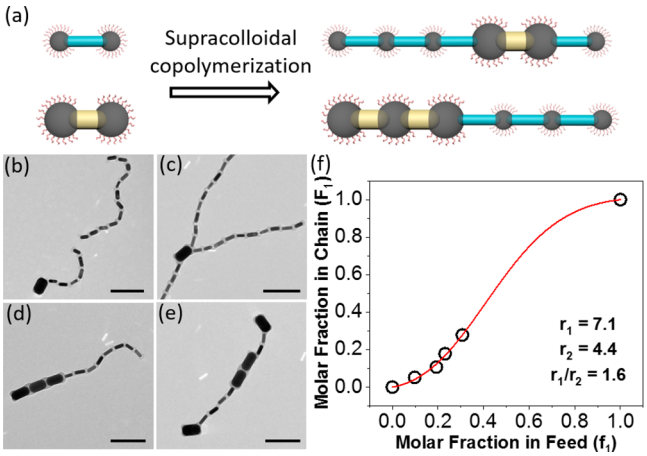

Figure 8. (a) Supracolloidal copolymerization of dumbbell-like AuNRs with two aspect ratios. (b–e) TEM images of copolymer nanorod chains prepared at different feeding ratios AuNR-1 (99.8 × 56.1 nm):AuNR-2 (59.4 × 15.9 nm): (b) 0.098; (c), 0.193; (d) 0.231; (e) 0.307. Scale bars are 200 nm. (f) Molar fraction in the chain (F_1) as a function of the molar fraction in the feed (f_1). The red curve is the fitting result using eq 1. F_1 was the statistical average from >2000 AuNRs from low-resolution TEM images.

would encounter a greater contribution to the minimization of surface energy.

CONCLUSIONS

In summary, we demonstrated a ligand deficiency exchange method to carry out site-specific surface modification of AuNRs by taking advantage of hydrophobicity-driven surface dewetting. Dumbbell-like AuNRs with selectively grafted polymer ligands at the two ends could be prepared by simply varying the concentration of water and hydrophobic PS_{169}-SH ligands in the presence of an amphiphilic BCP surfactant of PS_{40}-*b*-PEO_{114}. At C_{water} of 9 vol % in DMF, patchy AuNRs showed structural evolutions from core–shell to defective core–shell and to dumbbell nanostructures (<2.1 μM) at PS_{169}-SH concentrations from 5.7 μM to 0.71 μM. The surface dewetting occurred at a relatively low grafting density of ∼0.08 chains/nm^2. We further demonstrated that dumbbell-like AuNRs could polymerize to 1-D nanochains upon thermal activation of the end PS domain. At C_{water} of 9 vol %, 1-D nanochains were obtained through supracolloidal polymerization upon thermal annealing at 90 °C. Our time-dependence studies revealed that such supracolloidal polymerization follows the temperature–solvent superposition principle; in other words, the polymerization at a high C_{water} would need either longer activation time or higher temperature. The polymerized 1-D nanochains with an adjustable end-to-end distance showed length-dependent longitudinal plasmon coupling and propagation. Such a supracolloidal polymerization strategy further allowed us to study the colloidal copolymerization of two different building blocks. Our findings in this work provide a platform for the preparation of nanocomposites and are insightful for the supramolecular colloidal self-assembly.

METHODS

Synthesis of CTAC-Capped AuNRs. 365 mg of CTAB (365 mg) was dissolved in 9.9 mL of warm water in a 20 mL glass vial by stirring at 30 °C for 30 min to afford a clear and transparent solution. Then, 0.1 mL of $HAuCl_4$ aqueous solution (10 mg/mL) was slowly placed in the glass vial to afford a yellowish solution, and the resulting solution was stirred at 30 °C for another 10 min. 0.6 mL of freshly prepared $NaBH_4$ aqueous solution (0.01 M, 0.38 mg/mL) was mixed with 0.4 mL of DI water in another vial, which was quickly injected into the previous Au-CTAB solution with vigorous magnetic stirring (900 rpm), and the solution color changed from yellowish to brownish immediately. The seed solution was stirred at 400 rpm for 5 min and left at 30 °C for 2 h before use.

AuNRs with an aspect ratio of 3.9 were synthesized based on the following procedure. First, 12.3 g of CTAC and 3.086 g of sodium oleate (NaOL) were mixed with 1 L of DI water in an Erlenmeyer flask, which was put into a 70 °C water bath. The flask was heated at 70 °C for ∼20 min until CTAC and NaOL were totally dissolved. Then the water bath was removed, and the flask was allowed to cool to ∼30 °C. 12 mL of $AgNO_3$ aqueous solution (8 mM, 1.36 mg/mL) was added, and the mixture was kept undisturbed at 30 °C for 15 min. 19.7 mL of $HAuCl_4$ aqueous solution (10 mg/mL) was placed in the flask, which afforded a slightly yellowish solution. The solution was stirred at 30 °C for at least 150 min until it became colorless. 8 mL of concentrated HCl solution (37 wt %) was placed in the flask to adjust the pH. After stirring for another 15 min, 2.5 mL of AA aqueous solution (0.064 M, 11.27 mg/mL) was added, and the solution was stirred at 700 rpm for 1 min. Finally, 3.2 mL of the aforementioned seed solution was quickly placed in the flask, and the solution was vigorously stirred for 30 s. The flask was kept undisturbed at 30 °C for 12 h. The length and diameter of as-synthesized AuNRs were 59.4 ± 4.1 and 15.9 ± 1.2 nm, respectively. The final product was isolated by centrifugation at 8000 rpm for 20 min.

AuNRs with an aspect ratio of 1.78 were synthesized by using the same procedure as mentioned above except that the amount of HCl was increased to 10 mL while the volume of seeds was decreased to 1.6 mL. The length and diameter of as-synthesized AuNRs were 99.8 ± 6.0 and 56.1 ± 2.3 nm, respectively. The final product was isolated by centrifugation at 6000 rpm for 20 min.

Synthesis of PS_{169}-SH. PS_{169}-SH was obtained by the reduction of PS ending with a chain transfer group. RAFT agent 3-(benzylthiocarbonothioylthio)propanoic acid (BCTPA) was used in the controlled/living radical polymerization of styrene (St). 10.4 g of St (100 mmol, 200 equiv),16.4 mg of azobisisobutyronitrile (AIBN) (0.1 mmol, 0.2 equiv), 136 mg of BCTPA (0.5 mmol, 1 equiv), and 20 mL of anisole were mixed in a 50 mL flask, which was purged with N_2 for 30 min. Then the reaction was carried out at 90 °C for 24 h. PS-BCTPA was obtained by precipitating the polymer solution in excess ethanol. The unreacted monomer and anisole were removed by two rounds of consecutive precipitation.

The synthesized PS_{169}-BCTPA was reduced under a N_2 atmosphere to afford PS-SH. 1 g of PS-BCTPA was dissolved in 24 mL of chloroform, which was followed by purging with N_2 for 15 min. Then, 2 mL of *n*-butylamine was slowly added to the polymer solution. The aminolysis of PS-BCTPA was carried out at room temperature for 2 h until the yellow color completely diminished. The polymer solution was concentrated, and the product was purified by three precipitations using excess ethanol.

Preparation of Patchy AuNRs. A one-pot ligand exchange method was used to prepare patchy AuNRs, where PS_{165}-SH and PS_{40}-b-PEO_{114} were used as the ligand and amphiphilic BCP surfactant, respectively. Various amounts of PS_{165}-SH (M_n= 17 kg/mol, $Đ$ = 1.2 and 2.1 μM), 2 mg of PS_{40}-b-PEO_{114} (M_n = 9.2 kg/mol, $Đ$ = 1.1 and 54 μM), and DMF were mixed in a 4 mL glass vial to make the total volume of solution precisely 2 mL. For the surface modification of CTAC-AuNRs, 40 mL of AuNRs (8 mg) was first centrifuged at 8000 rpm for 20 min to remove excess CTAC ligands. The supernatant was discarded, and the sediments were redispersed into 15 mL of DI water. Then 3 mL of concentrated AuNR aqueous solution (1.6 mg) was centrifuged for a second time, and the precipitates were collected with a total volume of ∼8 μL, which were quickly injected into the above 2 mL of polymer solution with gentle shaking. The vial was capped and sonicated for 5 min. The solution was incubated at RT for 4 h without any disturbance. Then 9 vol % of H_2O (0.2 mL) was added, and the mixture was further sonicated for 4

https://doi.org/10.1021/acsnano.3c03929
ACS Nano 2023, 17, 12788–12797

min. The solution was annealed in an oil bath at 90 °C for 20 min. For purification and characterization, 0.2 mL of the solution was injected into 1 mL of DI water followed by the addition of 10 mg (25 mM) of CTAC as the compensatory ligand. The solution was further centrifuged twice to remove the free polymer. The nanorod chain aqueous solution is stable at RT for months; however, it caused fast precipitation without the addition of external CTAC before purification. For patchy AuNRs with different surface coverages, like core−shell, dumbbell, or nanorod chains, the procedures stated above were almost identical except the amount of PS_{17k}-SH or the water content was adjusted accordingly as described in the main text.

Supracolloidal Copolymerization. The colloidal copolymerization of AuNRs with different aspect ratios (3.9 and 1.8) was carried out in DMF/water (91/9, vol %) mixed solvent at 90 °C. Various amounts of PS-SH-modified AuNRs (M_1) were centrifuged and added to a DMF/water solution containing a constant M_2, and then the mixture of two monomer solutions was sonicated for 2 min and thermally annealed at 90 °C for 20 min. Afterward, the nanochains were quenched by water containing 25 mM of CTAC, which was then purified by centrifugation and characterized by TEM.

ASSOCIATED CONTENT

Supporting Information

The Supporting Information is available free of charge at https://pubs.acs.org/doi/10.1021/acsnano.3c03929.

Detailed experimental procedures, synthesis of polymers and AuNRs, characterization methods, additional electron microscope images, analysis, grafting density calculations, and UV−vis absorption spectra (PDF)

AUTHOR INFORMATION

Corresponding Author

Jie He − *Polymer Program, Institute of Materials Science, and Department of Chemistry, University of Connecticut, Storrs, Connecticut 06269, United States;* orcid.org/0000-0003-0252-3094; Email: jie.he@uconn.edu

Authors

Hanyi Duan − *Polymer Program, University of Connecticut, Storrs, Connecticut 06269, United States;* orcid.org/0000-0001-8720-2761

Zhenyang Jia − *Department of Chemical and Biomolecular Engineering, Rice University, Houston, Texas 77005, United States;* orcid.org/0000-0002-7795-7180

Maham Liaqat − *Department of Chemistry, University of Connecticut, Storrs, Connecticut 06269, United States*

Matthew D. Mellor − *Department of Chemistry, University of Connecticut, Storrs, Connecticut 06269, United States*

Haiyan Tan − *Institute of Materials Science, University of Connecticut, Storrs, Connecticut 06269, United States*

Mu-Ping Nieh − *Polymer Program and Institute of Materials Science, University of Connecticut, Storrs, Connecticut 06269, United States;* orcid.org/0000-0003-4462-8716

Yao Lin − *Polymer Program, Institute of Materials Science, and Department of Chemistry, University of Connecticut, Storrs, Connecticut 06269, United States;* orcid.org/0000-0001-5227-2663

Stephan Link − *Department of Chemistry, Rice University, Houston, Texas 77005, United States;* orcid.org/0000-0002-4781-930X

Christy F. Landes − *Department of Chemical and Biomolecular Engineering and Department of Chemistry, Rice University, Houston, Texas 77005, United States;* orcid.org/0000-0003-4163-6497

Complete contact information is available at: https://pubs.acs.org/10.1021/acsnano.3c03929

Author Contributions

H.D., Y.L., and J.H. conceived the idea and designed the experiments. H.D. performed the experiments and collected the data. Z.J., S.L. and C.F.L. contributed to the single particle spectroscopy and data analysis. M.L., M.D.M., and H.T. contributed to the electron microscopic characterization. M-.P.N., Y.L., and J.H. supervised the project. H.D. and J.H. drafted the manuscript, and all authors contributed to finalizing the manuscript.

Notes

The authors declare no competing financial interest.

ACKNOWLEDGMENTS

This work was partially supported by the National Science Foundation (CHE-2102245) on polymer synthesis and the University of Connecticut through its REP program on self-assembly. C.F.L. acknowledges support from the Welch Foundation (Grant No. C-1787) and from the Kenneth S. Pitzer-Schlumberger Chair in Chemistry at Rice University. S.L. thanks the Robert A. Welch Foundation for support through the Charles W. Duncan, Jr.-Welch Chair in Chemistry (C-0002). TEM and SEM studies were performed using the facilities in the Bioscience Electron Microscopy Laboratory at the University of Connecticut and Thermo Fisher Scientific Center for Advanced Microscopy and Materials Analysis (CAMMA).

REFERENCES

(1) Glotzer, S. C. Some assembly required. *Science* **2004**, *306*, 419−420.

(2) Yi, C.; Liu, H.; Zhang, S.; Yang, Y.; Zhang, Y.; Lu, Z.; Kumacheva, E.; Nie, Z. Self-limiting directional nanoparticle bonding governed by reaction stoichiometry. *Science* **2020**, *369*, 1369−1374.

(3) Yi, C.; Yang, Y.; Liu, B.; He, J.; Nie, Z. Polymer-guided assembly of inorganic nanoparticles. *Chem. Soc. Rev.* **2020**, *49*, 465−508.

(4) Macfarlane, R. J. From Nano to Macro: Thinking Bigger in Nanoparticle Assembly. *Nano Lett.* **2021**, *21*, 7432−7434.

(5) Woessner, Z. J.; Skrabalak, S. E. Symmetry-Reduced Metal Nanostructures Offer New Opportunities in Plasmonics and Catalysis. *J. Phys. Chem. C* **2021**, *125*, 23587−23596.

(6) Vo, T.; Glotzer, S. C. A theory of entropic bonding. *Proc. Natl. Acad. Sci. U.S.A.* **2022**, *119*, No. e2116414119.

(7) Santos, P. J.; Gabrys, P. A.; Zornberg, L. Z.; Lee, M. S.; Macfarlane, R. J. Macroscopic materials assembled from nanoparticle superlattices. *Nature* **2021**, *591*, 586−591.

(8) Liu, W.; Tagawa, M.; Xin, H. L.; Wang, T.; Emamy, H.; Li, H.; Yager, K. G.; Starr, F. W.; Tkachenko, A. V.; Gang, O. Diamond family of nanoparticle superlattices. *Science* **2016**, *351*, 582−586.

(9) Cui, Y.; Wang, J.; Liang, J.; Qiu, H. Molecular Engineering of Colloidal Atoms. *Small* **2023**, *19*, 2207609.

(10) Huang, M.; Hsu, C.-H.; Wang, J.; Mei, S.; Dong, X.; Li, Y.; Li, M.; Liu, H.; Zhang, W.; Aida, T.; Zhang, W.-B.; Yue, K.; Cheng, S. Z. D. Selective assemblies of giant tetrahedra via precisely controlled positional interactions. *Science* **2015**, *348*, 424−428.

(11) Gan, Z.; Zhou, D.; Ma, Z.; Xu, M.; Xu, Z.; He, J.; Zhou, J.; Dong, X.-H. Local Chain Feature Mandated Self-Assembly of Block Copolymers. *J. Am. Chem. Soc.* **2023**, *145*, 487−497.

(12) Skrabalak, S. E. Symmetry in Seeded Metal Nanocrystal Growth. *Acc. Mater. Res.* **2021**, *2*, 621−629.

(13) Yang, T. H.; Shi, Y.; Janssen, A.; Xia, Y. Surface capping agents and their roles in shape-controlled synthesis of colloidal metal nanocrystals. *Angew. Chem., Int. Ed.* **2020**, *59*, 15378−15401.

(14) Bian, T.; Gardin, A.; Gemen, J.; Houben, L.; Perego, C.; Lee, B.; Elad, N.; Chu, Z.; Pavan, G. M.; Klajn, R. Electrostatic co-assembly of nanoparticles with oppositely charged small molecules into static and dynamic superstructures. *Nat. Chem.* **2021**, *13*, 940−949.
(15) Zhang, J.; Santos, P. J.; Gabrys, P. A.; Lee, S.; Liu, C.; Macfarlane, R. J. Self-Assembling Nanocomposite Tectons. *J. Am. Chem. Soc.* **2016**, *138*, 16228−16231.
(16) Glotzer, S. C.; Solomon, M. J. Anisotropy of building blocks and their assembly into complex structures. *Nat. Mater.* **2007**, *6*, 557−562.
(17) Sacanna, S.; Pine, D. J. Shape-anisotropic colloids: Building blocks for complex assemblies. *Curr. Opin. Colloid Interface Sci.* **2011**, *16*, 96−105.
(18) Zheng, Y.; Zhong, X.; Li, Z.; Xia, Y. Successive, Seed-Mediated Growth for the Synthesis of Single-Crystal Gold Nanospheres with Uniform Diameters Controlled in the Range of 5−150 nm. *Part Part Syst Charact* **2014**, *31*, 266−273.
(19) Jana, N. R.; Gearheart, L.; Murphy, C. J. Seeding Growth for Size Control of 5−40 nm Diameter Gold Nanoparticles. *Langmuir* **2001**, *17*, 6782−6786.
(20) Grzelczak, M.; Pérez-Juste, J.; Mulvaney, P.; Liz-Marzán, L. M. Shape control in gold nanoparticle synthesis. *Chem. Soc. Rev.* **2008**, *37*, 1783−1791.
(21) Murphy, C. J.; Sau, T. K.; Gole, A. M.; Orendorff, C. J.; Gao, J.; Gou, L.; Hunyadi, S. E.; Li, T. Anisotropic metal nanoparticles: synthesis, assembly, and optical applications. *J. Phys. Chem. B* **2005**, *109*, 13857−13870.
(22) Wang, C.; Daimon, H.; Sun, S. Dumbbell-like Pt-Fe3O4 Nanoparticles and Their Enhanced Catalysis for Oxygen Reduction Reaction. *Nano Lett.* **2009**, *9*, 1493−1496.
(23) Gilroy, K. D.; Ruditskiy, A.; Peng, H.-C.; Qin, D.; Xia, Y. Bimetallic nanocrystals: syntheses, properties, and applications. *Chem. Rev.* **2016**, *116*, 10414−10472.
(24) Yi, C.; Yang, Y.; Nie, Z. Alternating Copolymerization of Inorganic Nanoparticles. *J. Am. Chem. Soc.* **2019**, *141*, 7917−7925.
(25) Song, J.; Cheng, L.; Liu, A.; Yin, J.; Kuang, M.; Duan, H. Plasmonic vesicles of amphiphilic gold nanocrystals: self-assembly and external-stimuli-triggered destruction. *J. Am. Chem. Soc.* **2011**, *133*, 10760−10763.
(26) He, J.; Liu, Y.; Babu, T.; Wei, Z.; Nie, Z. Self-Assembly of Inorganic Nanoparticle Vesicles and Tubules Driven by Tethered Linear Block Copolymers. *J. Am. Chem. Soc.* **2012**, *134*, 11342−11345.
(27) He, J.; Huang, X.; Li, Y.-C.; Liu, Y.; Babu, T.; Aronova, M. A.; Wang, S.; Lu, Z.; Chen, X.; Nie, Z. Self-Assembly of Amphiphilic Plasmonic Micelle-Like Nanoparticles in Selective Solvents. *J. Am. Chem. Soc.* **2013**, *135*, 7974−7984.
(28) Song, J.; Lin, L.; Yang, Z.; Zhu, R.; Zhou, Z.; Li, Z.-W.; Wang, F.; Chen, J.; Yang, H.; Chen, X. Self-Assembled Responsive Bilayered Vesicles with Adjustable Oxidative Stress for Enhanced Cancer Imaging and Therapy. *J. Am. Chem. Soc.* **2019**, *141*, 8158−8170.
(29) Dong, W.; Zhang, Y.; Yi, C.; Chang, J. J.; Ye, S.; Nie, Z. Halogen Bonding-Driven Reversible Self-Assembly of Plasmonic Colloidal Molecules. *ACS Nano* **2023**, *17*, 3047−3054.
(30) Li, B.; Han, W.; Jiang, B.; Lin, Z. Crafting Threads of Diblock Copolymer Micelles via Flow-Enabled Self-Assembly. *ACS Nano* **2014**, *8*, 2936−2942.
(31) Li, B.; Jiang, B.; Han, W.; He, M.; Li, X.; Wang, W.; Hong, S. W.; Byun, M.; Lin, S.; Lin, Z. Harnessing Colloidal Crack Formation by Flow-Enabled Self-Assembly. *Angew. Chem., Int. Ed.* **2017**, *56*, 4554−4559.
(32) Jones, M. R.; Macfarlane, R. J.; Lee, B.; Zhang, J.; Young, K. L.; Senesi, A. J.; Mirkin, C. A. DNA-nanoparticle superlattices formed from anisotropic building blocks. *Nat. Mater.* **2010**, *9*, 913−917.
(33) Duan, H.; Yang, Y.; Zhang, Y.; Yi, C.; Nie, Z.; He, J. What is next in polymer-grafted plasmonic nanoparticles? *Giant* **2020**, *4*, 100033.
(34) Liu, Y.; Han, X.; He, L.; Yin, Y. Thermoresponsive Assembly of Charged Gold Nanoparticles and Their Reversible Tuning of Plasmon Coupling. *Angew. Chem., Int. Ed.* **2012**, *51*, 6373−6377.
(35) Liu, L.; Gao, Z.; Jiang, B.; Bai, Y.; Wang, W.; Yin, Y. Reversible assembly and dynamic plasmonic tuning of Ag nanoparticles enabled by limited ligand protection. *Nano Lett.* **2018**, *18*, 5312−5318.
(36) Sánchez-Iglesias, A.; Claes, N.; Solís, D. M.; Taboada, J. M.; Bals, S.; Liz-Marzán, L. M.; Grzelczak, M. Reversible clustering of gold nanoparticles under confinement. *Angew. Chem., Int. Ed.* **2018**, *130*, 3237−3240.
(37) Duan, H.; Lin, Y.; He, J. Metal nanoparticles grafted with polymeric ligands: Self-assembly guided by polymers in solution. In *Encyclopedia of Nanomaterials*, 1st edition; Yin, Y., Lu, Y., Xia, Y., Eds.; Elsevier: 2023; pp 390−406.
(38) Cai, Y.-Y.; Choi, Y. C.; Kagan, C. R. Chemical and Physical Properties of Photonic Noble-Metal Nanomaterials. *Adv. Mater.* **2022**, 2108104.
(39) Kim, J.-M.; Lee, C.; Lee, Y.; Lee, J.; Park, S.-J.; Park, S.; Nam, J.-M. Synthesis, Assembly, Optical Properties, and Sensing Applications of Plasmonic Gap Nanostructures. *Adv. Mater.* **2021**, *33*, 2006966.
(40) Lee, S.; Sim, K.; Moon, S. Y.; Choi, J.; Jeon, Y.; Nam, J.-M.; Park, S.-J. Controlled Assembly of Plasmonic Nanoparticles: From Static to Dynamic Nanostructures. *Adv. Mater.* **2021**, *33*, 2007668.
(41) Sánchez-Iglesias, A.; Grzelczak, M.; Altantzis, T.; Goris, B.; Pérez-Juste, J.; Bals, S.; Van Tendeloo, G.; Donaldson, S. H.; Chmelka, B. F.; Israelachvili, J. N.; Liz-Marzán, L. M. Hydrophobic Interactions Modulate Self-Assembly of Nanoparticles. *ACS Nano* **2012**, *6*, 11059−11065.
(42) Duan, H.; Malesky, T.; Wang, J.; Liu, C.-H.; Tan, H.; Nieh, M.-P.; Lin, Y.; He, J. Patchy metal nanoparticles with polymers: controllable growth and two-way self-assembly. *Nanoscale* **2022**, *14*, 7364−7371.
(43) Horsch, M. A.; Zhang, Z.; Glotzer, S. C. Self-Assembly of Polymer-Tethered Nanorods. *Phys. Rev. Lett.* **2005**, *95*, 056105.
(44) DeVries, G. A.; Brunnbauer, M.; Hu, Y.; Jackson, A. M.; Long, B.; Neltner, B. T.; Uzun, O.; Wunsch, B. H.; Stellacci, F. Divalent metal nanoparticles. *Science* **2007**, *315*, 358−361.
(45) Nagaoka, Y.; Zhu, H.; Eggert, D.; Chen, O. Single-component quasicrystalline nanocrystal superlattices through flexible polygon tiling rule. *Science* **2018**, *362*, 1396−1400.
(46) Zhang, N.-N.; Shen, X.; Liu, K.; Nie, Z.; Kumacheva, E. Polymer-Tethered Nanoparticles: From Surface Engineering to Directional Self-Assembly. *Acc. Chem. Res.* **2022**, *55*, 1503−1513.
(47) Zhou, J.; Creyer, M. N.; Chen, A.; Yim, W.; Lafleur, R. P. M.; He, T.; Lin, Z.; Xu, M.; Abbasi, P.; Wu, J.; Pascal, T. A.; Caruso, F.; Jokerst, J. V. Stereoselective Growth of Small Molecule Patches on Nanoparticles. *J. Am. Chem. Soc.* **2021**, *143*, 12138−12144.
(48) Tuff, W. J.; Hughes, R. A.; Golze, S. D.; Neretina, S. Ion Beam Milling as a Symmetry-Breaking Control in the Synthesis of Periodic Arrays of Identically Aligned Bimetallic Janus Nanocrystals. *ACS Nano* **2023**, *17*, 4050−4061.
(49) Li, B.; Jiang, B.; Tang, H.; Lin, Z. Unconventional seed-mediated growth of ultrathin Au nanowires in aqueous solution. *Chem. Sci.* **2015**, *6*, 6349−6354.
(50) Wang, F.; Cheng, S.; Bao, Z.; Wang, J. Anisotropic Overgrowth of Metal Heterostructures Induced by a Site-Selective Silica Coating. *Angew. Chem., Int. Ed.* **2013**, *52*, 10344−10348.
(51) Hinman, J. G.; Eller, J. R.; Lin, W.; Li, J.; Li, J.; Murphy, C. J. Oxidation State of Capping Agent Affects Spatial Reactivity on Gold Nanorods. *J. Am. Chem. Soc.* **2017**, *139*, 9851−9854.
(52) Kim, A.; Zhou, S.; Yao, L.; Ni, S.; Luo, B.; Sing, C. E.; Chen, Q. Tip-Patched Nanoprisms from Formation of Ligand Islands. *J. Am. Chem. Soc.* **2019**, *141*, 11796−11800.
(53) Xu, H.; Xu, Y.; Pang, X.; He, Y.; Jung, J.; Xia, H.; Lin, Z. A general route to nanocrystal kebabs periodically assembled on stretched flexible polymer shish. *Sci. Adv.* **2015**, *1*, No. e1500025.

https://doi.org/10.1021/acsnano.3c03929
ACS Nano 2023, 17, 12788−12797

(54) Pang, X.; He, Y.; Jung, J.; Lin, Z. 1D nanocrystals with precisely controlled dimensions, compositions, and architectures. *Science* **2016**, *353*, 1268−1272.
(55) Chen, T.; Yang, M.; Wang, X.; Tan, L. H.; Chen, H. Controlled Assembly of Eccentrically Encapsulated Gold Nanoparticles. *J. Am. Chem. Soc.* **2008**, *130*, 11858−11859.
(56) Liu, Y.; Klement, M.; Wang, Y.; Zhong, Y.; Zhu, B.; Chen, J.; Engel, M.; Ye, X. Macromolecular Ligand Engineering for Programmable Nanoprism Assembly. *J. Am. Chem. Soc.* **2021**, *143*, 16163−16172.
(57) Kim, A.; Vo, T.; An, H.; Banerjee, P.; Yao, L.; Zhou, S.; Kim, C.; Milliron, D. J.; Glotzer, S. C.; Chen, Q. Symmetry-breaking in patch formation on triangular gold nanoparticles by asymmetric polymer grafting. *Nat. Commun.* **2022**, *13*, 1−14.
(58) Nagaoka, Y.; Tan, R.; Li, R.; Zhu, H.; Eggert, D.; Wu, Y. A.; Liu, Y.; Wang, Z.; Chen, O. Superstructures generated from truncated tetrahedral quantum dots. *Nature* **2018**, *561*, 378−382.
(59) Grzelczak, M.; Sánchez-Iglesias, A.; Mezerji, H. H.; Bals, S.; Pérez-Juste, J.; Liz-Marzán, L. M. Steric Hindrance Induces crosslike Self-Assembly of Gold Nanodumbbells. *Nano Lett.* **2012**, *12*, 4380−4384.
(60) Liu, K.; Nie, Z.; Zhao, N.; Li, W.; Rubinstein, M.; Kumacheva, E. Step-Growth Polymerization of Inorganic Nanoparticles. *Science* **2010**, *329*, 197−200.
(61) Gao, B.; Arya, G.; Tao, A. R. Self-orienting nanocubes for the assembly of plasmonic nanojunctions. *Nat. Nanotechnol.* **2012**, *7*, 433−437.
(62) Hayes, O. G.; McMillan, J. R.; Lee, B.; Mirkin, C. A. DNA-Encoded Protein Janus Nanoparticles. *J. Am. Chem. Soc.* **2018**, *140*, 9269−9274.
(63) Lu, J.; Xue, Y.; Bernardino, K.; Zhang, N.-N.; Gomes, W. R.; Ramesar, N. S.; Liu, S.; Hu, Z.; Sun, T.; de Moura, A. F.; Kotov, N. A.; Liu, K. Enhanced optical asymmetry in supramolecular chiroplasmonic assemblies with long-range order. *Science* **2021**, *371*, 1368−1374.
(64) Zheng, J.; Cheng, X.; Zhang, H.; Bai, X.; Ai, R.; Shao, L.; Wang, J. Gold Nanorods: The Most Versatile Plasmonic Nanoparticles. *Chem. Rev.* **2021**, *121*, 13342−13453.
(65) Gao, J.; Bender, C. M.; Murphy, C. J. Dependence of the gold nanorod aspect ratio on the nature of the directing surfactant in aqueous solution. *Langmuir* **2003**, *19*, 9065−9070.
(66) He, J.; Wei, Z.; Wang, L.; Tomova, Z.; Babu, T.; Wang, C.; Han, X.; Fourkas, J. T.; Nie, Z. Hydrodynamically Driven Self-Assembly of Giant Vesicles of Metal Nanoparticles for Remote-Controlled Release. *Angew. Chem., Int. Ed.* **2013**, *125*, 2523−2528.
(67) Vigderman, L.; Khanal, B. P.; Zubarev, E. R. Functional gold nanorods: synthesis, self-assembly, and sensing applications. *Adv. Mater.* **2012**, *24*, 4811−4841.
(68) Caswell, K.; Wilson, J. N.; Bunz, U. H.; Murphy, C. J. Preferential end-to-end assembly of gold nanorods by biotin-streptavidin connectors. *J. Am. Chem. Soc.* **2003**, *125*, 13914−13915.
(69) Wang, L.; Zhu, Y.; Xu, L.; Chen, W.; Kuang, H.; Liu, L.; Agarwal, A.; Xu, C.; Kotov, N. A. Side-by-side and end-to-end gold nanorod assemblies for environmental toxin sensing. *Angew. Chem., Int. Ed.* **2010**, *122*, 5604−5607.
(70) Wang, Y.; DePrince, A. E., III; Gray, S. K.; Lin, X.-M.; Pelton, M. Solvent-Mediated End-to-End Assembly of Gold Nanorods. *J. Phys. Chem. Lett.* **2010**, *1*, 2692−2698.
(71) Nie, Z.; Fava, D.; Rubinstein, M.; Kumacheva, E. "Supramolecular" assembly of gold nanorods end-terminated with polymer "pom-poms": effect of pom-pom structure on the association modes. *J. Am. Chem. Soc.* **2008**, *130*, 3683−3689.
(72) Nie, Z.; Fava, D.; Kumacheva, E.; Zou, S.; Walker, G. C.; Rubinstein, M. Self-assembly of metal-polymer analogues of amphiphilic triblock copolymers. *Nat. Mater.* **2007**, *6*, 609−614.
(73) Yang, Y.; Yi, C.; Duan, X.; Wu, Q.; Zhang, Y.; Tao, J.; Dong, W.; Nie, Z. Block-Random Copolymer-Micellization-Mediated Formation of Polymeric Patches on Gold Nanoparticles. *J. Am. Chem. Soc.* **2021**, *143*, 5060−5070.
(74) Duan, H.; Luo, Q.; Wei, Z.; Lin, Y.; He, J. Symmetry-Broken Patches on Gold Nanoparticles through Deficient Ligand Exchange. *ACS Macro Lett.* **2021**, *10*, 786−790.
(75) Choueiri, R. M.; Galati, E.; Thérien-Aubin, H.; Klinkova, A.; Larin, E. M.; Querejeta-Fernández, A.; Han, L.; Xin, H. L.; Gang, O.; Zhulina, E. B.; Rubinstein, M.; Kumacheva, E. Surface patterning of nanoparticles with polymer patches. *Nature* **2016**, *538*, 79−83.
(76) Liu, B.; Thanneeru, S.; Lopes, A.; Jin, L.; McCabe, M.; He, J. Surface Engineering of Spherical Metal Nanoparticles with Polymers toward Selective Asymmetric Synthesis of Nanobowls and Janus-Type Dimers. *Small* **2017**, *13*, 1700091.
(77) Zhu, H.; Fan, Z.; Song, S.; Eggert, D.; Liu, Y.; Shi, W.; Yuan, Y.; Kim, K.-S.; Grünwald, M.; Chen, O. Dual Atomic Coherence in the Self-Assembly of Patchy Heterostructural Nanocrystals. *ACS Nano* **2022**, *16*, 15053−15062.
(78) Yang, S.; LaCour, R. A.; Cai, Y.-Y.; Xu, J.; Rosen, D. J.; Zhang, Y.; Kagan, C. R.; Glotzer, S. C.; Murray, C. B. Self-Assembly of Atomically Aligned Nanoparticle Superlattices from Pt-Fe3O4 Heterodimer Nanoparticles. *J. Am. Chem. Soc.* **2023**, *145*, 6280−6288.
(79) Chen, G.; Gibson, K. J.; Liu, D.; Rees, H. C.; Lee, J.-H.; Xia, W.; Lin, R.; Xin, H. L.; Gang, O.; Weizmann, Y. Regioselective surface encoding of nanoparticles for programmable self-assembly. *Nat. Mater.* **2019**, *18*, 169−174.
(80) Zou, R.; Zhang, Q.; Zhao, Q.; Peng, F.; Wang, H.; Yu, H.; Yang, J. Thermal stability of gold nanorods in an aqueous solution. *Colloids Surf. A: Physicochem. Eng. Asp.* **2010**, *372*, 177−181.
(81) Ye, X.; Gao, Y.; Chen, J.; Reifsnyder, D. C.; Zheng, C.; Murray, C. B. Seeded Growth of Monodisperse Gold Nanorods Using Bromide-Free Surfactant Mixtures. *Nano Lett.* **2013**, *13*, 2163−2171.
(82) Liu, K.; Lukach, A.; Sugikawa, K.; Chung, S.; Vickery, J.; Therien-Aubin, H.; Yang, B.; Rubinstein, M.; Kumacheva, E. Copolymerization of Metal Nanoparticles: A Route to Colloidal Plasmonic Copolymers. *Angew. Chem., Int. Ed.* **2014**, *53*, 2648−2653.
(83) Huang, Z.; Raciti, D.; Yu, S.; Zhang, L.; Deng, L.; He, J.; Liu, Y.; Khashab, N. M.; Wang, C.; Gong, J.; Nie, Z. Synthesis of Platinum Nanotubes and Nanorings via Simultaneous Metal Alloying and Etching. *J. Am. Chem. Soc.* **2016**, *138*, 6332−6335.
(84) Qiu, J.; Xie, M.; Lyu, Z.; Gilroy, K. D.; Liu, H.; Xia, Y. General Approach to the Synthesis of Heterodimers of Metal Nanoparticles through Site-Selected Protection and Growth. *Nano Lett.* **2019**, *19*, 6703−6708.
(85) Byers, C. P.; Hoener, B. S.; Chang, W.-S.; Yorulmaz, M.; Link, S.; Landes, C. F. Single-Particle Spectroscopy Reveals Heterogeneity in Electrochemical Tuning of the Localized Surface Plasmon. *J. Phys. Chem. B* **2014**, *118*, 14047−14055.
(86) Collins, S. S. E.; Searles, E. K.; Tauzin, L. J.; Lou, M.; Bursi, L.; Liu, Y.; Song, J.; Flatebo, C.; Baiyasi, R.; Cai, Y.-Y.; Foerster, B.; Lian, T.; Nordlander, P.; Link, S.; Landes, C. F. Plasmon Energy Transfer in Hybrid Nanoantennas. *ACS Nano* **2021**, *15*, 9522−9530.
(87) Slaughter, L. S.; Wu, Y.; Willingham, B. A.; Nordlander, P.; Link, S. Effects of Symmetry Breaking and Conductive Contact on the Plasmon Coupling in Gold Nanorod Dimers. *ACS Nano* **2010**, *4*, 4657−4666.
(88) Prodan, E.; Radloff, C.; Halas, N. J.; Nordlander, P. A Hybridization Model for the Plasmon Response of Complex Nanostructures. *Science* **2003**, *302*, 419−422.
(89) Slaughter, L. S.; Willingham, B. A.; Chang, W.-S.; Chester, M. H.; Ogden, N.; Link, S. Toward Plasmonic Polymers. *Nano Lett.* **2012**, *12*, 3967−3972.
(90) Odian, G., *Principles of Polymerization*; Wiley: 2004.

https://doi.org/10.1021/acsnano.3c03929
ACS Nano 2023, 17, 12788−12797